Acta Biomaterialia 9 (2013) 8972–8982

Contents lists available at SciVerse ScienceDirect

Acta Biomaterialia

journal homepage: www.elsevier.com/locate/actabiomat

Silk hydrogels from non-mulberry and mulberry silkworm cocoons processed with ionic liquids

Simone S. Silva [a,b,*], Elena G. Popa [a,b], Manuela E. Gomes [a,b], Mariana B. Oliveira [a,b], Sunita Nayak [c], Bano Subia [c], João F. Mano [a,b], Subhas C. Kundu [c,*], Rui L. Reis [a,b]

[a] 3B's Research Group – Biomaterials, Biodegradables and Biomimetics, University of Minho, Headquarters of the European Institute of Excellence on Tissue Engineering and Regenerative Medicine, AvePark, Zona Industrial da Gandra, Caldas das Taipas, 4806-909 Guimarães, Portugal
[b] ICVS/3B's – PT Government Associate Laboratory, Braga/Guimarães, Portugal
[c] Department of Biotechnology, Indian Institute of Technology, Kharagpur 721302, India

ARTICLE INFO

Article history:
Received 20 February 2013
Received in revised form 21 June 2013
Accepted 26 June 2013
Available online 9 July 2013

Keywords:
Bombyx mori
Fibroin
Antheraea mylitta
Ionic liquids
Hydrogels

ABSTRACT

Matrices based on silk fibroin from the non-mulberry silkworm *Antheraea mylitta* and the mulberry silkworm *Bombyx mori* have demonstrated good applicability in regenerative medicine. However, the cocoons of *A. mylitta* are underutilized in part due to their lack of solubility in traditional organic solvents. Therefore, the present work investigates the solubilization and processing of degummed fibers obtained from the cocoons of both silkworm species into hydrogels using ionic liquids (ILs). The developed hydrogels exhibited a rubbery consistency, viscoelastic behavior and rapid degradation in the presence of protease XIV. Scanning electron and confocal microscopy images suggest that human adipose stem cells (hASCs) are able to adhere to and migrate at different levels within the hydrogel structures. Moreover, the MTS assay demonstrated the maintenance of cell metabolic activity for up to 28 days, while DNA quantification showed that hASCs were able to proliferate on the seeded hydrogels. The findings indicate that complete IL removal from the fabricated hydrogels results in a positive hASCs cellular response. Thus the present approach provides a unique opportunity to broaden the processability and application of silk fibroin obtained from *A. mylitta* cocoons for regenerative medicine, namely cartilage regeneration.

1. Introduction

Recent investigations have shown that matrices based on silk fibroin from the non-mulberry silkworm *Antheraea mylitta* and the mulberry silkworm *Bombyx mori* have diverse morphologies, controllable degradation and good biocompatibility [1–4]. Because of their versatility and properties silks are used as a biomaterial for biomedical, biotechnological and tissue engineering applications [1,5]. Silk protein fibroin obtained from the non-mulberry Indian tropical tasar silkworm *A. mylitta* is utilized as a promising biomaterial for tissue engineering and biomedical applications due to its biocompatibility, biodegradability and mechanical stability [6,7]. The non-mulberry Indian tropical tasar silkworm *A. mylitta* silk protein fibroin has a molecular weight of 395 kDa, with two subunits each of approximately 197 kDa [6,8]. The additional feature of *A. mylitta* silk fibroin is the presence of arginine–glycine–aspartic acid (RGD) motifs, integrin binding sites for cell attachment, proliferation and differentiation [8]. The presence of RGD motifs on *A. mylitta*-based matrices provide a substrate for fibroblasts, chondrocytes, the osteogenic differentiation of human mesenchymal stem cells (hMSCs), rat bone marrow stromal cells (BSCs), and cardiomyocytes [6,7,9]. Thus silk fibroin from the non-mulberry fed *A. mylitta* and mulberry fed *B. mori* differ not only in their amino acid composition but also in the presence/absence of integrin binding RGD sequences [10,11].

On the other hand, previous studies conducted with silk fibroin showed that hydrogel formation and the sol–gel transition were dependent on protein concentration, temperature, and pH, among other parameters [12–16]. Different methods of silk-based hydrogel formation, for example using carbon dioxide and chemical crosslinking, have been investigated [3,17,18]. Silk hydrogels have been previously characterized and investigated for pancreatic islets co-encapsulated with extracellular matrix (ECM) proteins and mesenchymal stromal cells [19]. Silk hydrogel-based delivery of bone morphogenetic protein for the treatment of large bone defects has been also investigated [20]. Despite promising findings on the use of *A. mylitta* fibroin protein isolated from the silk gland their cocoons are still underutilized, in part due to their insolubility in

* Corresponding authors at: 3Bs Research Group- Biomaterials, Biodegradables and Biomimetics, University of Minho, Headquarters of the European Institute of Excellence on Tissue Engineering and Regenerative Medicine, AvePark, Zona Industrial da Gandra, Caldas das Taipas, 4806-909 Guimarães, Portugal (S.S. Silva), Department of Biotechnology, Indian Institute of Technology Kharagpur, India (S. C. Kundu).

E-mail addresses: simonesilva@dep.uminho.pt (S.S. Silva), kundu@hijli.iitkgp.ernet.in (S.C. Kundu).

1742-7061/$ - see front matter © 2013 Acta Materialia Inc. Published by Elsevier Ltd. All rights reserved.
http://dx.doi.org/10.1016/j.actbio.2013.06.044

water and the usual organic solvents. Earlier reports emphasized the use of certain ionic liquids (ILs) [21] to solubilize *B. mori* protein fibroin, alone [22,23] or combined with chitosan [24]. To our knowledge, to date only one report on the use of ILs as a solvent for *Antheraea assamensis* silk fibroin has been described [25]. However, no work has been reported involving ILs in the dissolution and processing of *A. mylitta* silk fibroin. In spite of the widespread application of ILs as templates and solvents for different biomacromolecules such as silk fibroin, chitin, and cellulose [24,26,27], issues concerning cellular response have not yet been fully explored. The present work reports the viability of silk protein fibroins obtained from the cocoons of non-mulberry fed *A. mylitta* and mulberry fed *B. mori* through dissolution and their processability as hydrogels using an IL, 1-butyl-3-methyl imidazolium acetate (BMIAc). The fabricated silk hydrogels were characterized biochemically and biophysically. The use of mesenchymal stem cells (MSCs) is an important tool in tissue engineering and regenerative medicine, mainly due to their plasticity and easy availability [28]. MSCs can be obtained from many tissues, for example bone marrow and adipose tissue, and are recognized as a potential cell substitute for chondrocytes in cartilage regeneration [29]. MSCs have been used to evaluate the cellular response of fabricated silk matrices, including hydrogels. An in vitro assessment was performed using human adipose-derived stem cells (hASCs) to validate the use of both fabricated silk hydrogels for cartilage regeneration. The main advantage of the present approach is that it provides a unique opportunity to broaden the application of Indian tasar silkworm *A. mylitta* fibroin obtained from cocoons for cartilage regeneration.

2. Materials and methods

2.1. Materials

Silk fibroin from cocoons of *B. mori* was kindly supplied by the APPACDM (Castelo Branco, Portugal). The silk cocoons of *A. mylitta* were obtained from IIT Kharagpur (West Bengal, India). The IL BMIAc (Sigma Aldrich) was chosen as solvent and used without further purification. All other chemicals were reagent grade and were used as received.

2.2. Methods

2.2.1. Isolation of silk protein fibroin from A. mylitta

Silk protein fibroin was isolated from cocoons of *A. mylitta* following a standard extraction protocol [30]. Briefly, cocoons were cut into small pieces, boiled in 0.02 M Na_2CO_3 for 45–60 min and washed with deionized water several times to remove sericin from the silk fibers. The degummed fibers were then dried completely at room temperature.

2.2.2. Isolation of silk protein fibroin from B. mori

The degumming process was achieved by boiling the silk from *B. mori* filaments for 1 h in water containing 1.1 g l^{-1} Na_2CO_3, followed by 30 min in water with 0.4 g l^{-1} Na_2CO_3 [17,31]. Finally, the resulting fibroin filaments were extensively rinsed in boiling distilled water and air dried at room temperature.

2.2.3. Preparation of the silk fibroin-based hydrogels

To prepare the hydrogels degummed fibers of cocoons of *A. mylitta* were dissolved in BMIAc at 95 °C at a concentration of 10 wt.%. The degummed fibers from *B. mori* were also dissolved using the same procedure. Both systems were kept under stirring for 8 h. After dissolution the fiber/IL solutions were transferred to polystyrene molds, followed by gelation at 4 °C overnight. The gelation process was completed by immersion of the molds in ethanol to obtain silk hydrogels, identified as AM and BM, from *A. mylitta*/IL and *B. mori*/IL solutions, respectively. The BMIAc removal procedure was carried out by immersing the materials in ethanol for 24 h, followed by Soxhlet extraction with ethanol for 5 days. During solvent removal aliquots of ethanol were collected for conductivity analysis. The conductivities of the aliquots of ethanol were measured using a conductivimeter (inoLab Multilevel 3) with a Sonda WTW TetraCon 325 detector. After IL removal the samples were treated with methanol/water (80/20 vol.%) for 30 min to for induce formation of beta-sheets.

2.3. Characterization

2.3.1. Biochemical and biophysical characterization

The amino acid composition of the samples, degummed fibroin from *A. mylitta* filaments, degummed fibroin from *B. mori* filaments, AM hydrogel and BM hydrogel, were performed after hydrolysis and derivatization, followed by analysis in a Waters 600 HPLC gradient system equipped with a Waters 2487 UV detector.

2.3.2. Fourier transform infrared (FTIR) spectroscopy

The infrared spectra of the silk structures were obtained with a Shimadzu-IR Prestige 21 spectrometer in the spectral region 4000–650 cm^{-1}, with a resolution of 2 cm^{-1} for 32 scans. FTIR spectra were obtained from the freeze-dried hydrogels to minimize the effect of the presence of water. After that the samples were powdered, mixed with KBr and processed into pellets. Fourier self-deconvolution (FSD) of the infrared spectra covering the amide I region (1595–1705 cm^{-1}) was performed using Origin® Software. To measure the relative areas of the amide I components FSD spectra were curve fitted to Gaussian line shape profiles. The deconvoluted amide I spectra were area normalized and the relative areas of the single bands were used to determine the fraction of the secondary structural elements. The band assignments and the detailed procedure to determine β-sheet crystallinity were described previously by Hu et al. [32].

2.3.3. Scanning electron microscopy (SEM)

Freeze-dried hydrogel samples were observed using a Leica Cambridge S360 scanning electron microscope. The materials were fixed using mutual conductive adhesive tape on aluminum stubs and covered with gold palladium using a sputter coater.

2.3.4. Differential scanning calorimetry (DSC)

DSC measurements were performed using a TA instruments DSC Q100 equipped with a cooling accessory to quantitatively characterize the bound and bulk water in the hydrogels. Approximately 10 mg of hydrogel was transferred to a DSC aluminum pan. Subsequently the pan was first cooled to −40 °C and then heated to 40 °C at a rate of 5 °C min^{-1} [16]. The linear baseline to integrate peaks was determined, and then the melting temperature (T_m) and enthalpy of fusion (ΔH) were calculated from the DSC thermograms using TA instruments software.

2.3.5. Dynamical mechanical analysis

Viscoelastic measurements of the AM and BM hydrogels were performed using a TRITEC2000B DMA from Triton Technology (UK) in compression mode. The hydrogels were always analyzed under hydrated conditions through immersion of the samples in a Teflon reservoir containing phosphate-buffered saline (PBS), used during all analysis periods. After equilibration at 37 °C the DMA spectra were obtained over a frequency scan of 0.1–10 Hz. The experiments were performed under a constant strain amplitude (30 μm). The average value of four tests is reported for each sample.

2.3.6. In vitro degradation

In vitro degradation of the silk hydrogels (AM and BM) was evaluated for 28 days using protease XIV from *Streptomyces griseus* with an activity of 4.5 U ml^{-1}. Silk hydrogels measuring 6.5 mm in diameter, 4.5 mm in height were immersed in 5 ml of PBS containing 2 U ml^{-1} protease enzyme. The samples were also incubated in PBS without enzyme under similar conditions for comparison. All systems were maintained at 37 °C. The enzyme solution was replaced with freshly prepared solution every 7 days to maintain the activity of the enzyme. Samples were collected at different time points, washed gently with distilled water, dried at 40 °C and weighed. Percentage weight loss at respective time points was calculated.

2.3.7. Human adipose stem cell isolation and expansion

hASCs were obtained from subcutaneous fat tissue, under protocols established with the Plastic Surgery Department of the Hospital da Prelada (Porto, Portugal) and isolated by enzymatic digestion as previously described [33]. Briefly, the adipose tissue samples were digested with 0.075% collagenase type II (Col II) (C6885, Sigma) in PBS (21600-044, Invitrogen) for 45 min at 37 °C under gentle stirring. The digested tissue was filtered with a 100 μm filter mesh, and centrifuged at 1000*g* for 10 min at 5 °C. Afterwards the cell suspension was washed for 10 min with lysis buffer (155 mM NH_4Cl, 10 mM $KHCO_3$, 0.1 mM EDTA = 14.61 mg, pH 7.3), to remove erythrocytes, and additionally centrifuged at 800*g* for 10 min at 5 °C. The adherent hASCs were expanded in basal medium with minimum essential medium (α-MEM) (12000-063, Invitrogen) with 10 vol.% fetal bovine serum (FBS) (10270, Invitrogen), 1 vol.% antibiotic–antimycotic and 2.2 mg ml^{-1} $NaHCO_3$ (S5761, Sigma) with medium changes every 3–4 days. Cells were subcultured at a cell density of 3.5×10^3 cells cm^{-2} until a sufficient cell number was achieved for use in the experimental assays.

2.3.7.1. Cell seeding. Prior to the cell culture studies the hydrogels were sterilized in an autoclave. The hASCs were seeded at a density of 3×10^5 cells cm^3 onto silk hydrogel samples with a diameter of 7 mm and a height of 5 mm. All seeded hydrogels were subsequently cultured for 28 days in either basal or chondrogenic medium in a 37 °C humidified atmosphere including 5% CO_2. The chondrogenic induction medium was composed of Dulbecco's modified Eagle's medium–low glucose (DMEM) (D5523, Sigma) supplemented with 3.8 mg ml^{-1} $NaHCO_3$, 1 vol.% antibiotic–antimycotic solution, 5 vol.% FBS (SH3007103, Fisher Scientific), 1× ITS + 1 (insulin–transferrin–selenium liquid medium supplement, I2521, Sigma), 17 mM L-ascorbic acid (A4544, Sigma), 0.1 M sodium pyruvate (P4562, Sigma), 35 mM L-proline (P5607, Sigma), 1 mM dexamethasone (D2915, Sigma) and 10 ng ml^{-1} human transforming growth factor-β1 (TGF-β1) (14-8348, eBioscience). Controls consisted of cell-seeded silk hydrogels cultured in basal medium (without chondrogenic growth factor) and silk hydrogels without cells, maintained in culture for the same time periods under the same cell maintenance conditions. The culture medium was replaced twice per week. At the end of each culture time point the samples were retrieved, rinsed with PBS and evaluated in terms of cellular behavior, by confocal analysis, MTS test, DNA quantification and histological evaluation.

2.3.7.2. Morphological analysis. The cell distribution and attachment of hASC cells on both the AM and BM constructs was analyzed using confocal microscopy. The matrices were fixed with 10% formalin for 30 min and then the samples were incubated with 1% bovine serum albumin (BSA) for 30 min. The constructs were permeabilized using 0.1% Triton X-100 for 5 min, then incubated with rhodamine–phalloidin for 20 min at room temperature, followed by washing with PBS and staining with 5 μg ml^{-1} Hoechst 33342 for 30 min. Fluorescence images from stained constructs were obtained using a confocal laser scanning microscope (Olympus FV1000). The morphology of the constructs was also observed using a Leica Cambridge S360 scanning electron microscope. The constructs were fixed using mutual conductive adhesive tape on aluminum stubs and covered with gold palladium using a sputter coater.

2.3.7.3. Viability and proliferation of human adipose-derived stem cells. The metabolic activity of hASCs seeded on the silk hydrogels was evaluated using the CellTiter 96® AQueous One Solution Cell Proliferation Assay (MTS, Promega). Briefly, cell–hydrogel constructs were placed in a mixture containing serum-free cell culture medium and MTS reagent at a 5:1 ratio and incubated for 3 h, at the end of which the optical density was read (OD 490 nm). Cell quantification was performed using the fluorimetric PicoGreen double-stranded DNA assay according to the manufacturer's instructions (Quant-iT™ PicoGreen® dsDNA Kit, P7589, Invitrogen). Briefly, cell–hydrogel constructs, collected after each time period, were rinsed with PBS, placed in microtubes containing 1 ml of ultra-pure water and stored at −80 °C until analyzed. The fluorescence of the samples was measured with a microplate reader (Synergie HT, Izasa) at 480 and 520 nm, and the DNA concentration was calculated using a standard curve (0–2 μg ml^{-1}) relating the amount of dsDNA to the fluorescence intensity.

2.3.7.4. Histological evaluation. Samples collected at the end of the culturing period were fixed with 3.7 vol.% formalin solution and stored at 4 °C until analysis. The samples were processed through a series of dehydration steps, embedded in paraffin (Microm EC350-2, Thermo Scientific) and sectioned at 3 μm (Microm HM 355, Thermo Scientific). For hematoxylin and eosin (H&E) staining the sections were colored with Papanicolaou Harris hematoxylin (05-12011/L, Bio-optica) for 3 min, washed in running tap water and stained with Eosin-Y (05-M10003, Bio-optica) for 30 s. Toluidine blue staining was used to evaluate cartilage ECM component deposition, namely glycosaminoglycans (GAGs). Toluidine blue staining solution was prepared by dissolving 1% toluidine blue in distilled water containing 0.5 g sodium borate (Riedelde-Haën). After filtering the solution the sections were dipped for 2–3 s. Finally, the slides were dehydrated through an alcohol series from 30 to 100 vol.% alcohol. The stained cells were visualized by reflected/transmitted light microscopy (Zeiss, Germany) and images were taken using a digital camera (Axion MRc5, Zeiss).

2.3.7.5. Immunohistochemical analysis. The tissue slides were deparaffinized and an antigen retrieval step was performed (the slides were dipped in 10 mM citrate buffer for 20 min at 95 °C). Next the sections were washed in PBS and endogenous peroxidase activity was quenched with 0.3% hydrogen peroxide (31642, Sigma) for 5–15 min. Sections were washed with PBS and blocked with 2.5% horse serum from a R.T.U. Vectastain® Universal Elite ABC Kit (PK-7200, Vector Laboratories) for 1 h to avoid non-specific staining. The samples were then incubated with rabbit anti-collagen I antibody (ab292, Abcam) and rabbit anti-collagen II antibody (ab34712, Abcam) for 1 h at room temperature in a humidified atmosphere. Next the slides were incubated with secondary antibody for 1 h at room temperature and developed with a DAB substrate kit for peroxidase (SK-4100, Vector Laboratories). Slides were counterstained with hematoxylin, mounted and visualized under a light microscope.

2.4. Statistical analysis

All quantitative experiments were run in triplicate and the results are expressed as means ± standard deviation for $n = 3$. Statistical analysis of the data was conducted by two-way ANOVA with Bonferroni's post test using GraphPadPrism v. 5.0 for Windows (GraphPad Software, San Diego, http://www.graphpad.com). Differences between the groups at $p < 0.05$ were considered to be statistically significant.

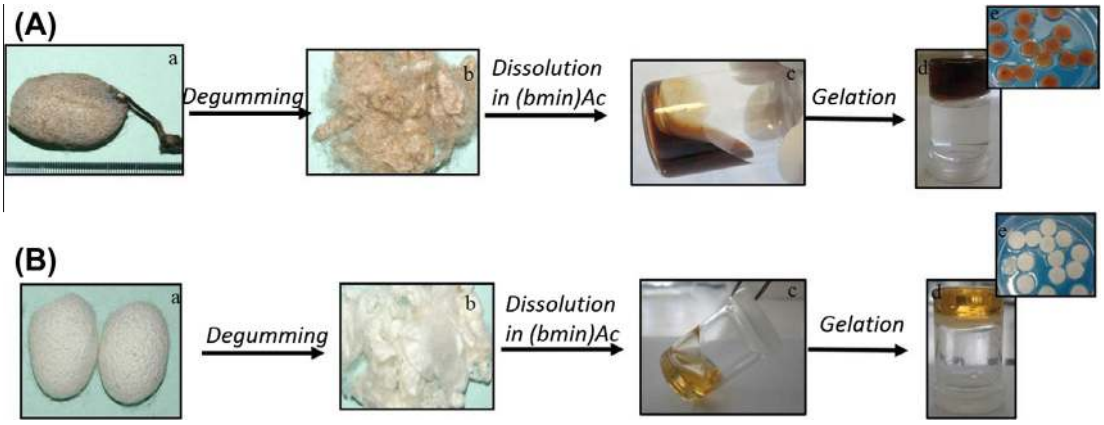

Fig. 1. Schematic representation of fabrication of silk hydrogels from non-mulberry and mulberry silk cocoons using BMIAc as solvent. (A): (a) *Antheraea mylitta* cocoons; (b) degummed fibers; (c) silk/BMIAc solution; (d) gelation of the silk/BMIAc solution; (e) fabricated hydrogels of *A. mylitta* (AM). (B): (a) *Bombyx mori* cocoons; (b) degummed fibers; (c) silk/BMIAc solution; (d) gelation of the silk/BMIAc solution; (e) fabricated hydrogels of *B. mori* (BM).

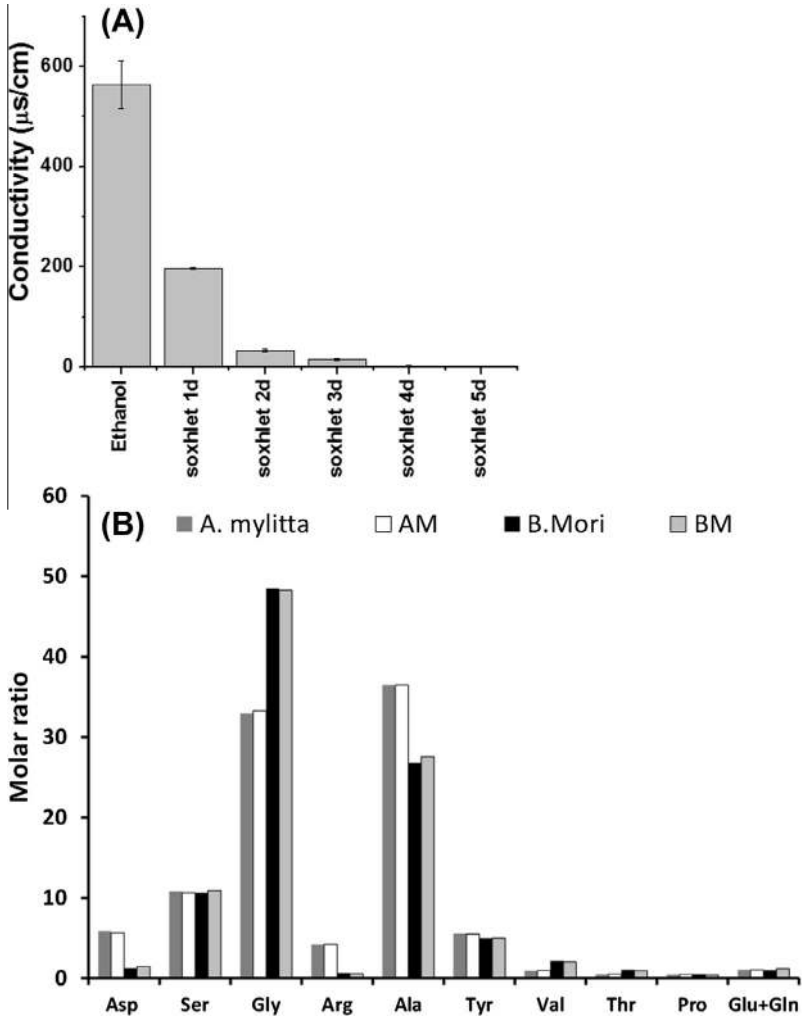

Fig. 2. (A) Conductivity measurements on aliquots of ethanol obtained after immersion of the structures in ethanol and soxhlet extraction. (B) Amino acid composition of the degummed fibers (*A. mylitta* and *B. mori*) and fabricated hydrogels (BM and AM).

3. Results and discussion

Efficient dissolution and processing of silk fibroin from *A. mylitta* and *B. mori* cocoons was achieved using BMIAc at a concentration of 10 wt.% (see Fig. 1). Both fibroin/BMIAc solutions were colorless and viscous even at high silk concentrations (10 wt.%). They also showed good stability over a long period (1–2 weeks in an inert atmosphere). Despite the broad applicability of silk fibroin obtained from *A. mylitta* (Fig. 1Aa)[2,34,35], the degummed fibers show a lack of solubility in common solvents such as lithium bromide, probably due to hydrogen bonding and the hydrophobic nature of the fibroin [36]. Some studies [22,24] have suggested that BMIAc is a good solvent for biomacromolecules like *B. mori* silk fibroin. However, to date the use of BMIAc in the dissolution of fibroin from cocoons of *A. mylitta* has not been described in the literature. Considering that *A. mylitta* cocoons are an underutilized material with a substantial amount of fibroin the present approach allows the dissolution and processing of *A. mylitta* degummed fibers with different shapes on the medium/large scale, increasing their applicability.

Upon cooling both viscous silk/BMIAc solutions resulted in the formation of gels (ionogels), which were molded into a cylindrical shape and subsequently immersed in an ethanol bath. The formation of silk hydrogels from aqueous solutions can be affected by the temperature, pH, and protein concentration [37]. In our approach silk gelation was influenced by reducing the temperature during molding and immersion in an ethanol bath. A similar temperature effect was observed for the gelation of chitosan–silk/BMIAc solutions [24]. The mechanism of gelation of silk/IL solutions can be associated with the formation of ionogels during cooling of the solutions. In an ionogel the IL is immobilized in a way that involves the formation of a three-dimensional (3-D) network that is responsible for the solid-like behavior of the material [38,39]. Also, the effect of temperature on the gelation response of the polymer/IL solutions could depend on the chemical structure of the chosen IL [21]. The mechanism of gelation of silk fibroin occurs through an association of intra–intermolecular interactions, including hydrophobic interactions and hydrogen bonds, which lead to physical crosslinking. In our case BMIAc could be immobilized in the gel matrix though specific interactions such as, for example, hydrogen bonds, hydrophobic interactions, etc., between silk chains and IL anions. This effect has an important role in gelling and the solid-like network of the resulting matrices. Both fabricated hydrogels had a rubbery consistency and a smooth and homogeneous surface (Fig. 1). Nevertheless, the BM hydrogels had better mechanical stability and consistency than the AM hydrogels.

The application of an IL in the fabrication of biomaterials would require its removal from the final material, since toxicity assays have shown that many commonly used ILs exhibit toxicity [40]. On the other hand, ILs have excellent ionic conductivity above their decomposition temperature [21]. Considering these, complete gelation and IL removal from the materials was initiated by immersion of the gels in pure ethanol, chosen as a good solvent for the IL [26]. Subsequently the materials were submitted to Soxhlet extraction with ethanol for 5 days. An evaluation of the efficiency of BMIAc removal from the materials during Soxhlet extraction was made through conductivity measurements. Fig. 2 shows the progressive decrease in conductivity during the extraction process. BMIAc was considered to have been almost totally removed from the silk hydrogels when the conductivity of the ethanol aliquots dropped below 0.5 $\mu S\ cm^{-1}$, indicating that the fabricated hydrogels had a low level of toxicity. In previous studies [26] high L929 cell viability was observed when using IL solutions at low concentration (1.69 and 4.23×10^{-3} g ml^{-1}), and consequently with low conductivity values, suggesting that IL removal from the material is an important step in obtaining a positive biological response.

The amino acid compositions of both the degummed fibers and hydrogels were investigated by HPLC analysis. Fig. 2B shows the

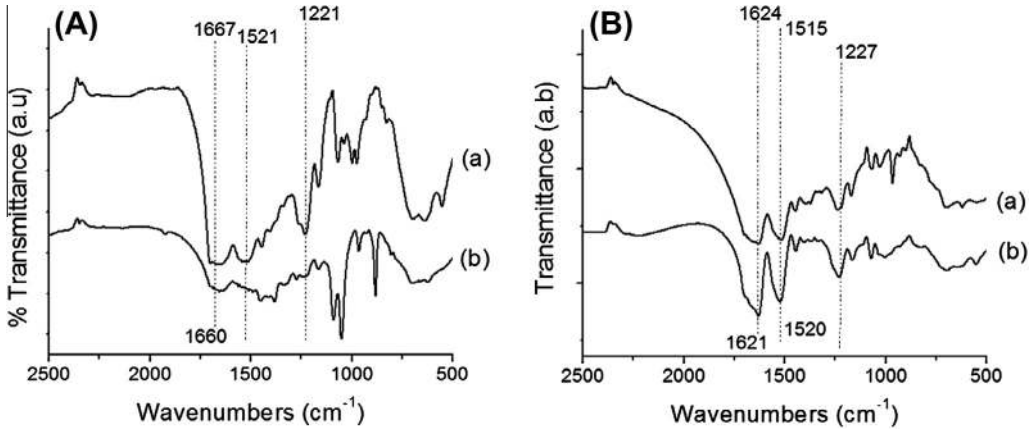

Fig. 3. (A) FTIR spectra of (a) a degummed *B. mori* fiber and (b) a degummed *A. mylitta* fiber. (B) FTIR spectra of (a) an AM and (b) a BM.

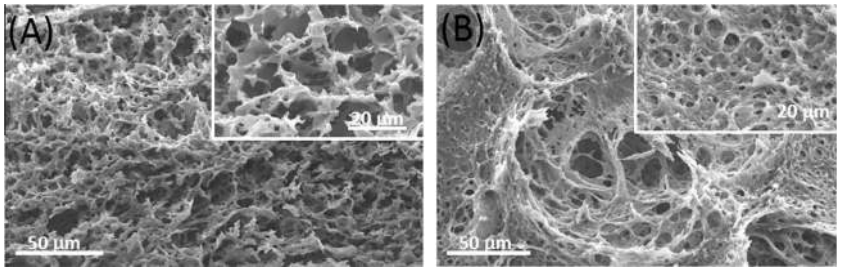

Fig. 4. SEM images of cross-sections of freeze-dried samples: (A) AM; (B) BM.

amino acids present in the degummed fibers and hydrogels (AM and BM). According to the literature [12] the primary structure of *B. mori* silk fibroin consists of the amino acid sequence glycine–serine–glycine–alanine–glycine–alanine, which is in agreement with the obtained amino acid composition (Fig. 2B). The obtained amino acid sequence of the degummed *A. mylitta* fiber is also in agreement with the findings reported by Datta et al. [8]. *A. mylitta* fibroin is predominantly constituted of alanine, glycine and serine amino acids [8]. It also contains a number of RGD sequences that are known to be effective in integrin-mediated cell attachment (AAN28165.1) [8]. By comparison, degummed *A. mylitta* fibers have higher arginine and alanine content than degummed *B. mori* fibers.

Some studies have indicated that the degumming conditions for silk fibroin protein could affect not only the mechanical properties but also cell function [41,42]. Following these studies we calculated the ratio of the molar concentrations of serine and glycine residues present in the degummed silk fibers in order to establish a metric for comparing the amino acid composition between samples. The values found were 0.22% and 0.33% for degummed *B. mori* and *A. mylitta* fibroin, respectively. Comparison between a cited molar ratio value (0.19%) reported for a 100% silk fibroin sample [42] and those calculated for *B. mori* and *A. mylitta* fibroin confirmed that both fibers were degummed.

Additionally, some differences were found between the AM and BM hydrogels, associated with the silk source (*A. mylitta* and *B. mori*). In BM the amino acids together comprised 86.73% of the total cited amino acids. Besides the mentioned amino acids others such as tyrosine, aspartic acid, and arginine were also present, but at low levels. The large amounts of glycine, alanine, and serine contribute to the formation of β-sheet and hydrophobic blocks [43]. In AM the cited amino acids together comprised 80.41% of the total amino acids, with arginine and aspartic acid being 9.84%. If the total polar (Ser and Lys) and non-polar amino acids (Ala, Gly and Phe) were considered the percentages between samples also differed: 12.86% for BM vs. 11.70% for AM (polar fraction); 67.81% for BM vs. 60.51% for AM (non-polar fraction). These results suggest the possible presence of larger regions of hydrophobic domains in the heavy chain of BM hydrogels.

To investigate the structural transition of the silk proteins before and after dissolution in BMIAc samples were analyzed by FTIR (Fig. 3a and b) [44]. Both degummed fibers exhibited peaks centered at 1221, 1521 and 1667 cm^{-1}, corresponding to amide I, II, and III, respectively (Fig. 3a) [44]. These peaks constitute the typical random coil conformation. After dissolution in BMIAc and methanol treatment the silk-based matrices showed peaks at 1624–1621 (amide I) and 1521 (amide II) cm^{-1}, which are

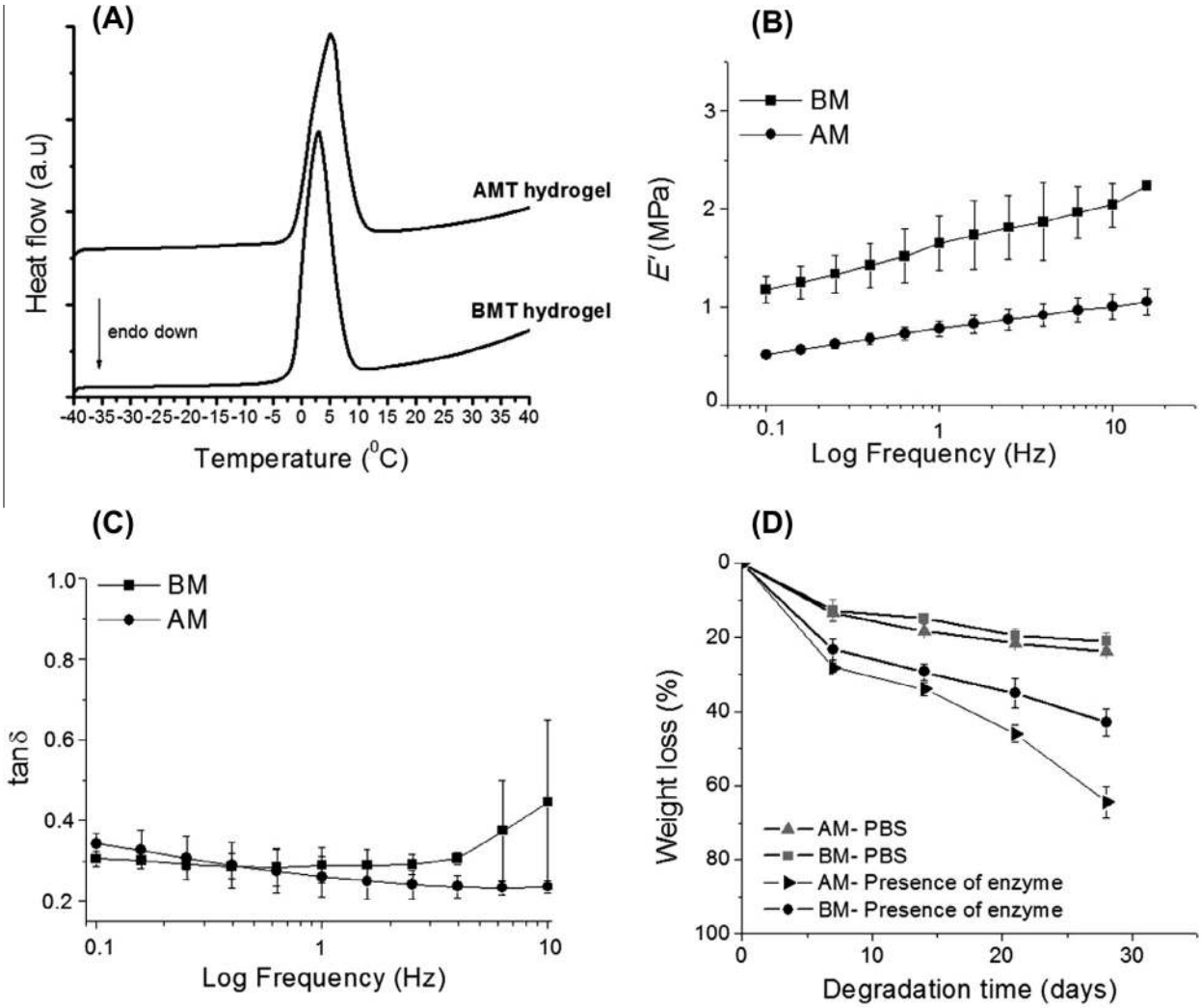

Fig. 5. (A) DSC endothermic profiles of silk hydrogels (AM and BM). Evaluation of the viscoelastic properties of the BM and AM hydrogels using DMA. (B) storage modulus (E') and (C) loss factor (tanδ). Frequency scans were performed in the range 0.1–10 Hz under wet conditions at 37 °C. (D) Degradation profile of the hydrogels (AM and BM) after immersion in PBS and in the presence of protease XIV for up to 28 days.

associated with intermolecular β-sheet bands (Fig. 3b) [24,35]. Absence of the characteristic peaks of BMIAc [26] suggest that this solvent could be almost totally removed by Soxhlet extraction. Thus the structural features of both hydrogels revealed that the use of BMIAc did not affect the characteristic β-sheet formation induced by methanol treatment.

By analyzing curve fitting of the FTIR spectra (data not shown) of the amide I region between 1595 and 1705 cm^{-1} for both hydrogels, taking into consideration that the regions 1600–1640 and 1690–1705 cm^{-1} are associated with intermolecular β-sheet bands [32,45], the amount of secondary structure in the AM and BM hydrogels was determined. The results show that the BM samples have a higher β-sheet content (28.6%) than the AM samples (25.14%). Relatively little is known about the mechanisms of dissolution of biopolymers such as silk fibroin in ILs. Some studies have suggested that ILs disrupts the hydrogen bonding present in β-sheets [46], which in turn can affect the β-sheet content in the hydrogels. In fact, differences in β-sheet content between the AM and BM samples were found, supporting this statement.

Both the AM and BM hydrogels were freeze-dried to obtain scaffolds, whose morphologies were investigated by SEM (see Fig. 4A and B). By analyzing the morphology of the cross-sections of the freeze-dried hydrogels it was noted that they had a uniform porosity and pore size distribution in the range 10–50 μm. Nevertheless, the BM hydrogels appeared as a compact structure (Fig. 4B) compared with the AM hydrogels (Fig. 4A). Similar pore sizes were observed in the case of *B. mori* scaffolds produced using silk fibroin isolated from cocoons [47]. Furthermore, these freeze-dried structures were too fragile to handle (data not shown).

The state of the water in the resulting silk hydrogels was characterized (Fig. 5A) by DSC analysis. In the DSC profiles of both silk hydrogels a sharp peak around −1 to 1.5 °C was observed. According to the literature [48] bound (non-freezing) and bulk (freezing) water can be found in hydrogels. The relatively lower melting point of water in the DSC curves of the hydrogels could be associated with bound and free water. Considering the enthalpy of fusion (ΔH) of the water (bound and free) in the silk hydrogels, the calculated percentage water contents were 73.1 ± 5.1% and 80.4 ± 2.2% for AM and BM, respectively.

Fig. 5B and C presents the viscoelastic behavior of the hydrogels, with the storage (elastic) and loss (viscous) components of the complex modulus represented. The DMA results point to an increase in E' for both hydrogels (Fig. 5B), although a significant difference was observed between BM and AM. In silk fibroin the presence of β-sheets has a marked influence on their mechanical properties [5]. Thus the differences observed in the mechanical properties of AM and BM can be related to the different contents of β-sheet, as determined by deconvolution of their FTIR spectra. Thus the highest β-sheet content, calculated for BM hydrogels, allowed the formation of a more rigid network, which affected the mechanical properties. The influence of the hydrogel composition on the loss factor (tanδ) was also analyzed. The tanδ results indicate that the damping capability is not different for the two materials and does not depend on the frequency (Fig. 5C). The elastic modulus of

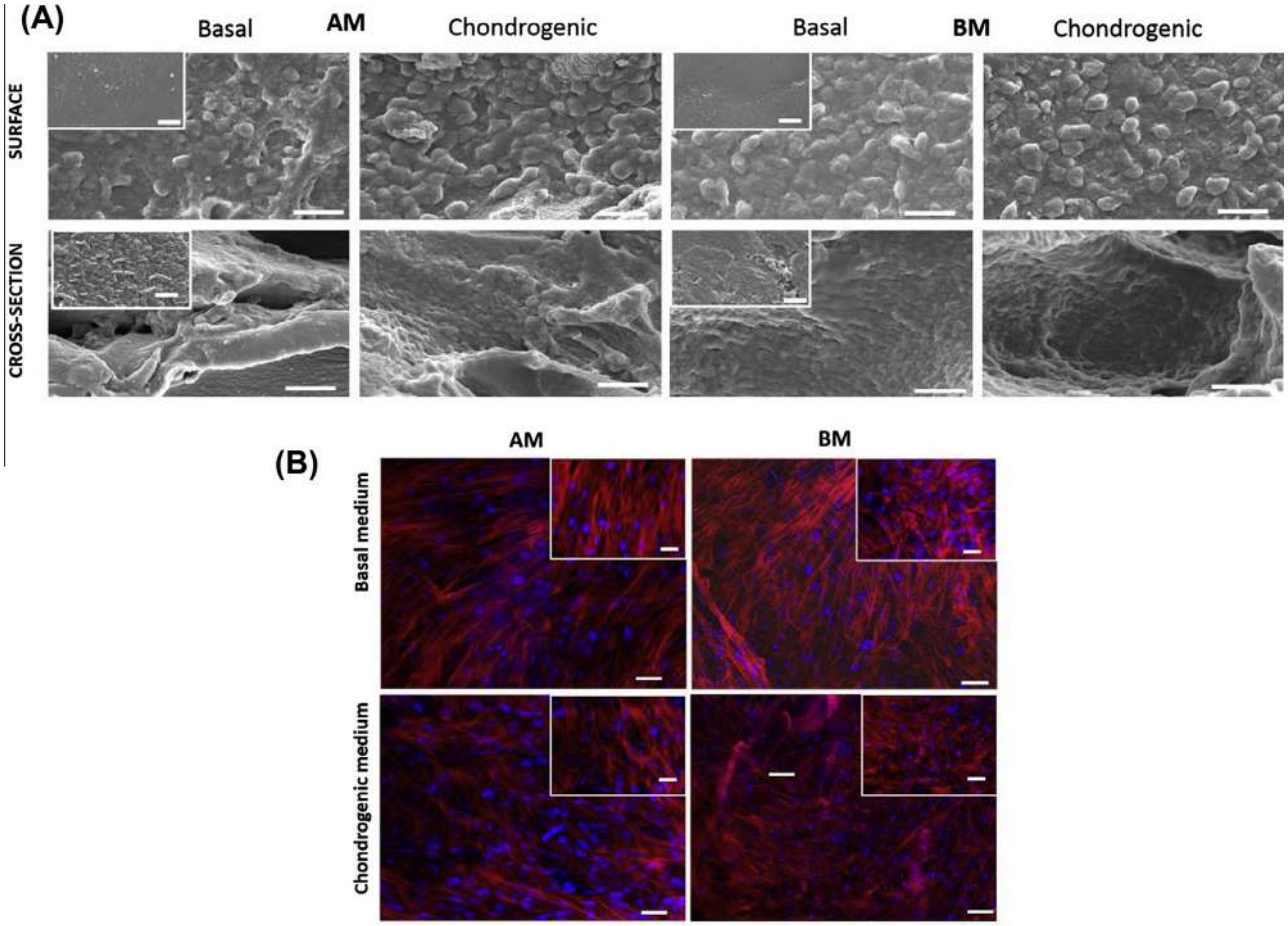

Fig. 6. (A) SEM images of hASCs seeded on both AM and BM hydrogels after 28 days. The upper left insets show SEM images of both hydrogels without cells. Scale bar 20 μm. (B) Confocal laser micrographs of hASCs cultured on AM and BM hydrogels after 28 days. The cells were stained with rhodamine–phalloidin for actin filaments (red) and Hoechst 33342 for nuclei. Scale bar: left, 20 μm; upper right, 20 μm.

human cartilage using conventional mechanical tests typically ranges from 0.45 to 0.8 MPa [49]. Comparing these values with the dynamic values herein obtained at a frequency of around 1 Hz, i.e. consistent with typical physiological movements such as walking, 0.88 MPa for AM and 1.7 MPa for BM, we conclude that the E' value obtained for AM is closer to the native cartilage value. Moreover, both biomaterials exhibited loss factor values higher than 0.2 over the complete range of frequencies, which shows clear viscoelastic behavior, i.e. an ability to absorb mechanical energy. This is an important characteristic of native cartilage, as well as of other tissues which are exposed to cyclical loading. Thus the mechanical properties of both the AM and BM hydrogels suggest that they are new options for application in the mentioned fields.

In vitro degradation of both hydrogels was investigated by monitoring the weight loss during incubation in PBS (Fig. 4C) and in the presence of protease XIV (Fig. 5D). Protease XIV was selected for use in the degradation assay on the basis of prior studies reported in the literature [50]. The degradation profile for both fabricated hydrogels (AM and BM) showed a controlled degradation rate in PBS with a weight loss of about 20% until the end of the incubation period. Proteolytic degradation of both hydrogels was faster in the presence of protease XIV (Fig. 5D). In particular, degradation was greater for AM hydrogels, with a weight loss of about 60% after 28 days. Furthermore, evident fragmentation of the matrices was observed when exposed to the enzyme, mainly of AM hydrogels, which started after 7 days and was prolonged up to 28 days. Fragmentation of the BM hydrogels was also evident, but to a lesser extent. The evident fragmentation of AM over time could involve a decrease in mechanical stability. The degradation rate of silk-based hybrid materials can be related to the β-sheet crystalline structure content within the bulk material [51]. Furthermore, the β-sheet region of silk fibroin is highly resistant to protease attack [52]. In that case the random coil region in silk fibroin is degraded, while the crystal region remains stable. The β-sheet content of the samples indicated that the BM samples had a higher value (28.6%) than the AM samples (25.14%). Thus the difference in resistance of the hydrogels to proteolytic degradation could be due to differences in β-sheet content. Thus the degradation/stability of the matrices could be associated with the processability of silk fibroin in ILs. Silk is defined by the US Pharmacopeia as non-degradable, since it retains greater than 50% of its tensile integrity 60 days post-implantation in vivo [5]. For instance, some researchers have reported that silk yarn does not degrade in PBS even after 10 weeks. Negligible degradation of a fibroin-based mesh 6 months after in vivo implantation has also been reported [53]. Thus the degradation patterns shown by both hydrogels (AM and BM) could be beneficial for tissue formation, specifically for cartilage repair.

The cellular responses to both hydrogels (AM and BM) were investigated to determine their potential as matrices of choice for cartilage repair using hASCs as a cell source. SEM observations (Fig. 6A) showed that hASCs are able to attach, proliferate and migrate at different levels within the inner sections of both silk hydrogels in basal and chondrogenic media. Cells appeared round in shape, with good attachment, as seen in chondrogenic medium, while in basal medium the cells look more spread for both formulations (Fig. 6A). In chondrogenic medium the cells cultured on hydrogels showed a round cell morphology typical of cartilage tissue, compared with the cells in basal medium which appeared more spindle-like in shape. These differences suggest that the cells were starting to differentiate to the chondrogenic phenotype. In the cross-sections the cells appeared to migrate at different levels within the inner sections of both silk hydrogels in basal and chondrogenic media, colonizing the entire space.

Cell attachment to the AM and BM hydrogels was also evaluated using confocal laser microscopy, with actin filaments represented in red and nuclei in blue (Fig. 6B). After 28 days culture in basal and chondrogenic media (supplemented with dexamethasone and TGF-β1) confocal images confirmed cell attachment with aligned actin filaments in all hydrogels (Fig. 6B). Highly magnified confocal images of cell seeded hydrogels are also presented. The AM hydrogel cultured in basal medium showed cells with straight actin filaments and round nuclei, while in the chondrogenic medium the cells formed a compact mesh with defined nuclei (Fig. 6B). hASCs in chondrogenic medium on BM hydrogels showed no well developed nuclei and non-aligned actin filaments, compared with AM under the same culture conditions. Overall, both the SEM and confocal images showed distinct cell morphologies for the two media, and a high degree of cell penetration with a cell distribution throughout the entire hydrogel structure for all tested conditions.

The metabolic activity of hASCs in the silk hydrogels (both AM and BM) increased during 28 days culture in basal medium. Statistical analysis of the data showed significant differences ($p < 0.01$ and $p < 0.05$) in metabolic activity between the longer term cultures of AM and BM hydrogels in basal medium. However, no significant statistical changes were registered in the metabolic activity of cell/hydrogel constructs exposed to chondrogenic medium (Fig. 7A).

The results of DNA quantification showed that hASCs in AM hydrogels cultured in basal medium were able to proliferate from the initial time point to 21 days, however a drop in the cellular content was seen (Fig. 7B). Furthermore, significant statistical differences ($p < 0.05$) between 21 and 28 days were observed in

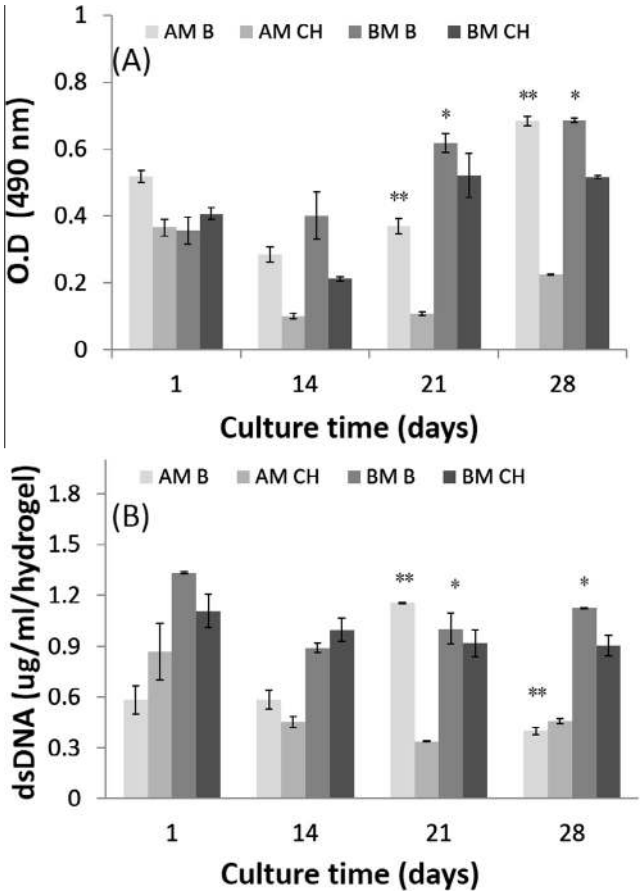

Fig. 7. (A) MTS results and (B) dsDNA content of hASCs seeded on both AM and BM hydrogels in basal (AM B and BM B) and chondrogenic media (AM CH and BM CH) as a function of culture time. Data represent means ± SD ($^{*}p \leqslant 0.05$, $^{**}p \leqslant 0.01$, two-way ANOVA).

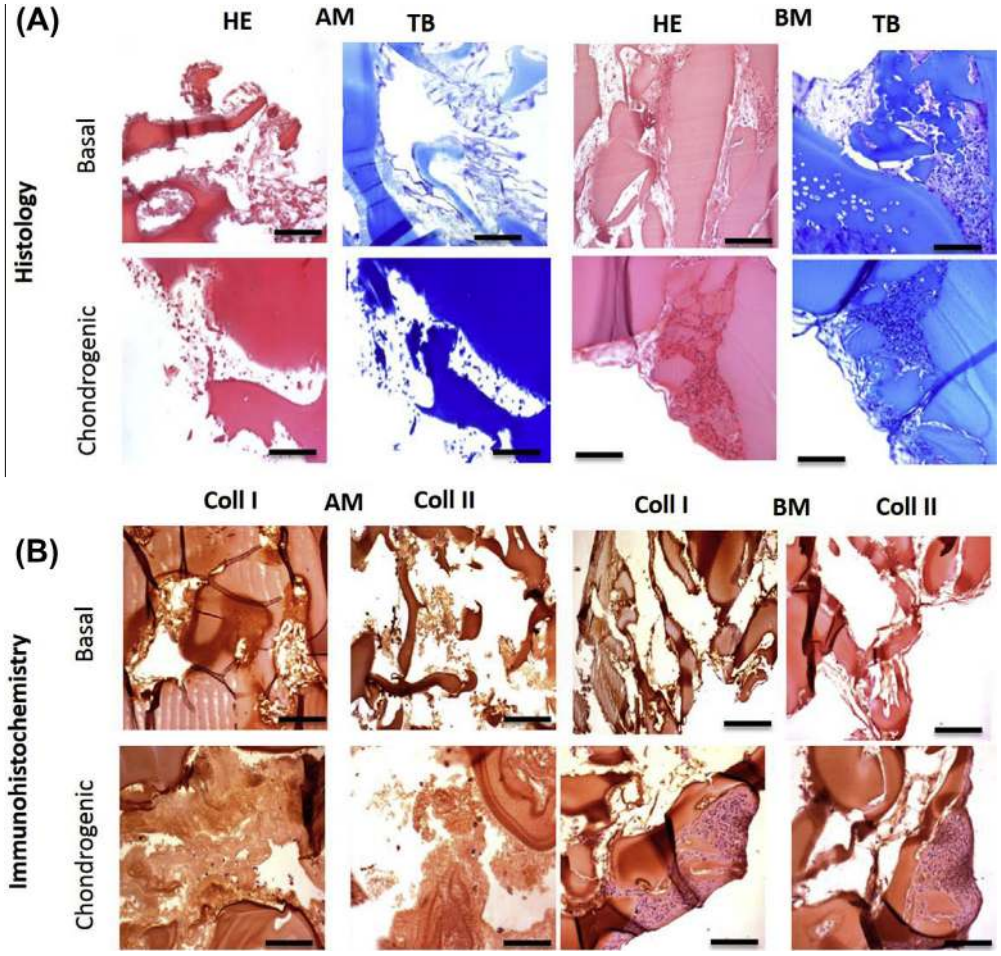

Fig. 8. (A) Histological staining of paraffin-embedded sections of hASC/BM hydrogel constructs after 28 days, stained with H&E (HE) and toluidine blue (TB). (B) Micrographs of cells and the matrix in BM hydrogels after 4 weeks culture. Immunohistochemical localization of Col I and Col II. Scale bar 100 μm.

BM/cell constructs cultured in basal medium. Both the metabolic activity and the proliferation assessment showed higher values in basal medium than in chondrogenic medium for the two hydrogels. This can be related to the fact that the stem cells are differentiating rather than proliferating. It is widely accepted that when cells differentiate the proliferation rate decreases [54]. Basal medium is usually used as an expansion medium, while the stimuli in the differentiation medium direct cells to a particular lineage. Generally it seems that the BM hydrogels induce a better cellular response compared with the AM hydrogels. This behavior could be related to the physical properties of the hydrogels, namely the stiffness and chemical composition of fibroin. The amino acid composition analyses performed on the hydrogels demonstrated that the fibroin obtained from cocoons of *A. mylitta* had similarities with that of the silk gland protein. Since RGD motifs on AM hydrogels were not identified a correlation between their presence and cellular performance cannot be made. Further studies on peptide mapping/protein/amino acid sequencing need to be performed to confirm the presence of RGD motifs in AM hydrogels. Also, the state of the water in the hydrogels could make a contribution to this finding. Based on DSC results, we can hypothesize that BM hydrogels could have more bound and free water than AM hydrogels, which in turn could accelerate cell adhesion protein interactions with the surface of the hydrogels, as reported by other studies [16].

The distribution of cells in the hydrogel constructs was observed through hematoxylin and eosin (H&E) staining. H&E analysis depicts a normal morphology of nuclei and cytoplasm in basal and chondrogenic medium for both hydrogels (Fig. 8A). Cartilage ECM components, negatively charged glycosaminoglycans (GAGs), were localized in cross-sections of hydrogels by toluidine blue staining (Fig. 8A). Owing to a higher cell density matrix development appeared to be greater in the BM hydrogels. Furthermore, a typical cartilage morphology, i.e. lacunae, was observed in BM hydrogels. The localization and distribution of cartilage-specific matrix proteins was evaluated by immunodetection (Fig. 8B). AM hydrogels showed few cells and specific cartilage protein staining was more evident in basal than in chondrogenic medium (Fig. 8B). The cartilage ECM components, collagen type I (Col I) and collagen type II (Col II), in BM silk hydrogels exposed to chondrogenic medium showed higher intensities compared with the basal medium. A higher cell density was observed under chondrogenic conditions, but it seems that no differences in staining for the two collagens were noted. The deposition of Col I and II proteins was higher in BM hydrogels, due to an increased cell distribution.

Histochemical analysis for sulfated GAGs indicated differences in the matrix deposition depending on the type of hydrogel (Fig. 8A). Localization of cartilage-specific components was greater in cells cultured in basal medium, suggesting that the 3-D environment was sufficient to stimulate ADSCs to develop typical characteristic, such as vacuoles and a round cell shape [55]. Furthermore, it can be clearly seen cells migrated inwards from the surface of BM hydrogels towards the middle (Fig. 8A), while in the AM hydrogels few cells are surrounded by matrix, interspersed between

short fragments of the hydrogels (Fig. 8A). Degradation of the matrices could happen during culture. For instance, it was observed that the AM hydrogels appeared more fragile with an open structure compared with the initial state. These features suggest that the hydrogels lose their stability due to degradation in culture medium, confirmed by the weight loss profile, with values between those in the presence or absence of enzyme (Fig. 4D). The differences in the degradation behavior, the state of the water present, the β-sheet content and the mechanical properties of the hydrogels could work together affecting the observed biological outcomes.

4. Conclusions

This work has proposed an alternative route to explore silk fibers (fibroins) obtained from *A. mylitta* and *B. mori* cocoons through their fabrication as hydrogels, using BMIAc. Both fabricated hydrogels had their own distinct properties, such as a controlled degradation rate, tuned mechanical properties, viscoelastic behavior, and bound water, which were dependent on the fibroin source. The biological evaluation suggested that hADSCs respond differently to the architecture of silk-based hydrogels. The development of a cartilage-specific matrix appears to depend on the structure, composition, stiffness, and state of the water present in the hydrogels. Thus the outcomes demonstrated herein suggest that the use of ILs for the dissolution/processing of degummed fibers derived from *A. mylitta* cocoons into hydrogels could be interesting in cartilage regeneration repair strategies. Furthermore, depending on the target tissue, the processing could be adapted, with the ILs being employed not only as solvent but also as reaction and hybridization medium. These opportunities will overcome the restricted use of fibroin from the silk glands of live silkworms.

Acknowledgments

The authors acknowledge financial support from the Portuguese Foundation for Science and Technology (Grants SFRH/BPD/45307/2008 and SFRH/BD/64070/2009), the Fundo Social Europeu, and the Programa Diferencial de Potencial Humano. This work was partially supported by the FEDER through POCTEP 0330_IBEROMARE_1_P and also by the Department of Biotechnology, Government of India. S.C.K. is grateful to R.L.R. and S.S.S. for their excellent hospitality during his stay at the 3B's laboratory, Guimarães, Portugal. R.L.R. also offers his sincere thanks to S.C.K. for providing hospitality during his short visits to his laboratory in the Indian Institute of Technology, Kharagpur.

Appendix A. Figures with essential color discrimination

Certain figures in this article, particularly Figures 1, 6 and 8, are difficult to interpret in black and white. The full colour images can be found in the on-line version, at http://dx.doi.org/10.1016/j.actbio.2013.06.044.

References

[1] Omenetto FG, Kaplan DL. New opportunities for an ancient material. Science 2010;329(5991):528–31.
[2] Acharya C, Ghosh SK, Kundu SC. Silk fibroin film from non-mulberry tropical tasar silkworms: a novel substrate for in vitro fibroblast culture. Acta Biomater 2009;5(1):429–37.
[3] Rockwood DN, Preda RC, Yucel T, Wang X, Lovett ML, Kaplan DL. Materials fabrication from *Bombyx mori* silk fibroin. Nat Protoc 2011;6(10):1612–31.
[4] Bhardwaj N, Kundu SC. Chondrogenic differentiation of rat MSCs on porous scaffolds of silk fibroin/chitosan blends. Biomaterials 2012;33(10):2848–57.
[5] Altman GH, Diaz F, Jakuba C, Calabro T, Horan RL, Chen J, et al. Silk-based biomaterials. Biomaterials 2003;24(3):401–16.
[6] Mandal BB, Kundu SC. A novel method for dissolution and stabilization of non-mulberry silk gland protein fibroin using anionic surfactant sodium dodecyl sulfate. Biotechnol Bioeng 2008;99(6):1482–9.
[7] Mandal BB, Das S, Choudhury K, Kundu SC. Implication of silk film RGD availability and surface roughness on cytoskeletal organization and proliferation of primary rat bone marrow cells. Tissue Eng A 2010;16(7):2391–403.
[8] Datta A, Ghosh AK, Kundu SC. Purification and characterization of fibroin from the tropical Saturniid silkworm, *Antheraea mylitta*. Insect Biochem Mol Biol 2001;31(10):1013–8.
[9] Patra C, Talukdar S, Novoyatleva T, Velagala SR, Mühlfeld C, Kundu B, et al. Silk protein fibroin from *Antheraea mylitta* for cardiac tissue engineering. Biomaterials 2012;33(9):2673–80.
[10] Datta A, Ghosh AK, Kundu SC. Differential expression of the fibroin gene in developmental stages of silkworm, *Antheraea mylitta* (Saturniidae). Comp Biochem Physiol B Biochem Mol Biol 2001;129(1):197–204.
[11] Minoura N, Aiba SI, Higuchi M, Gotoh Y, Tsukada M, Imai Y. Attachment and growth of fibroblast cells on silk fibroin. Biochem Biophys Res Commun 1995;208(2):511–6.
[12] Kim UJ, Park JY, Li CM, Jin HJ, Valluzzi R, Kaplan DL. Structure and properties of silk hydrogels. Biomacromolecules 2004;5(3):786–92.
[13] Nagarkar S, Nicolai T, Chassenieux C, Lele A. Structure and gelation mechanism of silk hydrogels. Phys Chem Chem Phys 2010;12(15):3834–44.
[14] Yucel T, Cebe P, Kaplan DL. Vortex-induced injectable silk fibroin hydrogels. Biophys J 2009;97(7):2044–50.
[15] Wang X, Kluge JA, Leisk GG, Kaplan DL. Sonication-induced gelation of silk fibroin for cell encapsulation. Biomaterials 2008;29(8):1054–64.
[16] Numata K, Katashima T, Sakai T. State of water, molecular structure, and cytotoxicity of silk hydrogels. Biomacromolecules 2011;12(6):2137–44.
[17] Silva SS, Motta A, Rodrigues MrT, Pinheiro AFM, Gomes ME, Mano JoF, et al. Novel genipin-cross-linked chitosan/silk fibroin sponges for cartilage engineering strategies. Biomacromolecules 2008;9(10):2764–74.
[18] Floren ML, Spilimbergo S, Motta A, Migliaresi C. Carbon dioxide induced silk protein gelation for biomedical applications. Biomacromolecules 2012;13(7):2060–72.
[19] Davis NE, Beenken-Rothkopf LN, Mirsoian A, Kojic N, Kaplan DL, Barron AE, et al. Enhanced function of pancreatic islets co-encapsulated with ECM proteins and mesenchymal stromal cells in a silk hydrogel. Biomaterials 2012;33(28):6691–7.
[20] Diab T, Pritchard EM, Uhrig BA, Boerckel JD, Kaplan DL, Guldberg RE. A silk hydrogel-based delivery system of bone morphogenetic protein for the treatment of large bone defects. J Mech Behav Biomed 2012;11:123–31.
[21] Anthony J, Brennecke J, Holbrey J, Maginn E, Mantz R, Trulove P, et al. Physicochemical properties of ionic liquids. In: Wasserscheid P, Welton T, editors. Ionic liquids in synthesis. Weinheim, Germany: Wiley-VCH; 2002.
[22] Gupta MK, Khokhar SK, Phillips DM, Sowards LA, Drummy LF, Kadakia MP, et al. Patterned silk films cast from ionic liquid solubilized fibroin as scaffolds for cell growth. Langmuir 2007;23(3):1315–9.
[23] Phillips DM, Drummy LF, Conrady DG, Fox DM, Naik RR, Stone MO, et al. Dissolution and regeneration of *Bombyx mori* silk fibroin using ionic liquids. J Am Chem Soc 2004;126(44):14350–1.
[24] Silva S, Santos T, Cerqueira M, Marques A, Reys L, Silva T, et al. The use of ionic liquids in the processing of chitosan/silk-based hydrogels for biomedical applications. Green Chem 2012;14:1463–70.
[25] Goujon N, Rajkhowa R, Wang X, Byrne N. Effect of solvent on ionic liquid dissolved regenerated *Antheraea assamensis* silk fibroin. J Appl Polym Sci 2013;128(6):4411–6.
[26] Silva SS, Duarte ARC, Carvalho AP, Mano JF, Reis RL. Green processing of porous chitin structures for biomedical applications combining ionic liquids and supercritical fluid technology. Acta Biomater 2011;7(3):1166–72.
[27] Swatloski RP, Spear SK, Holbrey JD, Rogers RD. Dissolution of cellulose with ionic liquids. J Am Chem Soc 2002;124(18):4974–5.
[28] Caplan AI. Adult mesenchymal stem cells for tissue engineering versus regenerative medicine. J Cell Physiol 2007;213(2):341–7.
[29] Csaki C, Schneider PRA, Shakibaei M. Mesenchymal stem cells as a potential pool for cartilage tissue engineering. Ann Anat 2008;190(5):395–412.
[30] Jin HJ, Park J, Karageorgiou V, Kim UJ, Valluzzi R, Cebe P, et al. Water-stable silk films with reduced β-sheet content. Adv Funct Mater 2005;15(8):1241–7.
[31] Silva SS, Maniglio D, Motta A, Mano JF, Reis RL, Migliaresi C. Genipin-modified silk-fibroin nanometric nets. Macromol Biosci 2008;8(8):766–74.
[32] Hu X, Kaplan D, Cebe P. Determining beta-sheet crystallinity in fibrous proteins by thermal analysis and infrared spectroscopy. Macromolecules 2006;39(18):6161–70.
[33] Rada T, Reis RL, Gomes ME. Adipose tissue-derived stem cells and their application in bone and cartilage tissue engineering. Tissue Eng B 2009;15(2):113–25.
[34] Acharya C, Ghosh S, Kundu S. Silk fibroin protein from mulberry and non-mulberry silkworms: cytotoxicity, biocompatibility and kinetics of L929 murine fibroblast adhesion. J Mater Sci Mater Med 2008;19(8):2827–36.
[35] Mandal BB, Kundu SC. Non-bioengineered silk gland fibroin protein: characterization and evaluation of matrices for potential tissue engineering applications. Biotechnol Bioeng 2008;100(6):1237–50.
[36] Kundu SC, Kundu B, Talukdar S, Bano S, Nayak S, Kundu J, et al. Invited review. Nonmulberry silk biopolymers. Biopolymers 2012;97(6):455–67.
[37] Matsumoto A, Chen J, Collette AL, Kim U-J, Altman GH, Cebe P, et al. Mechanisms of silk fibroin sol–gel transitions. J Phys Chem B 2006;110(43):21630–8.

[38] Le Bideau J, Viau L, Vioux A. Ionogels, ionic liquid based hybrid materials. Chem Soc Rev 2011;40(2):907–25.
[39] Néouze M-A, Bideau JL, Gaveau P, Bellayer S, Vioux A. Ionogels, new materials arising from the confinement of ionic liquids within silica-derived networks. Chem Mat 2006;18(17):3931–6.
[40] Zhao DB, Liao YC, Zhang ZD. Toxicity of ionic liquids. Clean Soil Air Water 2007;35(1):42–8.
[41] Jiang P, Liu H, Wang C, Wu L, Huang J, Guo C. Tensile behavior and morphology of differently degummed silkworm (*Bombyx mori*) cocoon silk fibres. Mater Lett 2006;60(7):919–25.
[42] Wray LS, Hu X, Gallego J, Georgakoudi I, Omenetto FG, Schmidt D, et al. Effect of processing on silk-based biomaterials: reproducibility and biocompatibility. J Biomed Mater Res B Appl Biomater 2011;99B(1):89–101.
[43] Jin H-J, Kaplan DL. Mechanism of silk processing in insects and spiders. Nature 2003;424(6952):1057–61.
[44] Um IC, Kweon H, Park YH, Hudson S. Structural characteristics and properties of the regenerated silk fibroin prepared from formic acid. Int J Biol Macromol 2001;29(2):91–7.
[45] Motta A, Maniglio D, Migliaresi C, Kim H-J, Wan X, Hu X, et al. Silk fibroin processing and thrombogenic responses. J Biomat Sci Polym E 2009;20(13):1875–97.
[46] Sah M, Pramanik K. Regenerated silk fibroin from *Bombyx mori* silk cocoon for tissue engineering applications. Int J Environ Sci Technol 2010;1(5):404–8.
[47] Nazarov R, Jin H-J, Kaplan DL. Porous 3-D scaffolds from regenerated silk fibroin. Biomacromolecules 2004;5(3):718–26.
[48] Hoffman AS. Hydrogels for biomedical applications. Adv Drug Deliv Rev 2002;54(1):3–12.
[49] Mansour JM. Kinesiology: the mechanics and pathomecanics of human movements. In: Oatis C, editor. Biomechanics of cartilage. Philadelphia, PA: Lippincott Williams and Wilkins; 2003. p. 66–79.
[50] Li M, Ogiso M, Minoura N. Enzymatic degradation behavior of porous silk fibroin sheets. Biomaterials 2003;24(2):357–65.
[51] Zhou J, Cao C, Ma X, Hu L, Chen L, Wang C. In vitro and in vivo degradation behavior of aqueous-derived electrospun silk fibroin scaffolds. Polym Degrad Stabil 2010;95(9):1679–85.
[52] Yongpei H, Qin Z, Renchuan Y, Lingshuang W, Mingzhong L. The relationship between secondary structure and biodegradation behavior of silk fibroin scaffolds. Adv Mater Sci Eng 2012;2012. p. 185905–10.
[53] Dal Pra I, Freddi G, Minic J, Chiarini A, Armato U. De novo engineering of reticular connective tissue in vivo by silk fibroin nonwoven materials. Biomaterials 2005;26(14):1987–99.
[54] Geoffrey MC. Cell proliferation in development and differentiation. In: The cell: a molecular approach. Sunderland, MA: Sinauer Associates; 2000.
[55] LeBaron RG, Athanasiou KA. Ex vivo synthesis of articular cartilage. Biomaterials 2000;21(24):2575–87.